Journal of Physics: Conference
Series

PAPER • **OPEN ACCESS**

Investigation of far-wake models coupled with yaw-induction control for power optimization

To cite this article: Kirby S. Heck *et al* 2024 *J. Phys.: Conf. Ser.* **2767** 092103

The Science of Making Torque from Wind (TORQUE 2024) IOP Publishing
Journal of Physics: Conference Series **2767** (2024) 092103 doi:10.1088/1742-6596/2767/9/092103

Investigation of far-wake models coupled with yaw-induction control for power optimization

Kirby S. Heck[1], Jaime Liew[1], Michael F. Howland[1]

[1]Civil and Environmental Engineering, Massachusetts Institute of Technology, Cambridge, MA 02139, USA

E-mail: mhowland@mit.edu

Abstract.

Combined wake steering and induction control is a promising strategy for increasing collective wind farm power production over standard turbine control. However, computationally efficient models for predicting optimal control set points still need to be tested against high-fidelity simulations, particularly in regimes of high rotor thrust. In this study, large eddy simulations (LES) are used to investigate a two-turbine array using actuator disk modeling in conventionally neutral atmospheric conditions. The thrust coefficient and yaw-misalignment angle are independently prescribed to the upwind turbine in each simulation while downwind turbine operation is fixed. Analyzing the LES velocity fields shows that near-wake length decreases and wake recovery rate increases with increasing thrust. We model the wake behavior with a physics-based near-wake and induction model coupled with a Gaussian far-wake model. The near-wake model predicts the turbine thrust and power depending on the wake steering and induction control set point. The initial wake velocities predicted by the near-wake model are validated against LES data, and a calibrated far-wake model is used to estimate the power maximizing control set point and power gain. Both model-predicted and LES optimal set points exhibit increases in yaw angle and thrust coefficient for the leading turbine relative to standard control. The model-optimal set point predicts a power gain of 18.1% while the LES optimal set point results in a power gain of 20.7%. In contrast, using a tuned cosine model for the power-yaw relationship results in a set point with a lower magnitude of yaw, a thrust coefficient lower than in standard control, and predicts a power gain of 13.7%. Using the physics-based, model-predicted set points in LES results in a power within 1.5% of optimal, showing potential for joint yaw-induction control as a method for predictably increasing wind farm power output.

1 Introduction

Wind farm flow control strategies, such as wake steering and induction control, intentionally operate upstream turbines in suboptimal conditions to increase total farm power relative to standard turbine control [1]. Wake steering redirects wakes by introducing a yaw-misalignment angle (γ) at the rotor with respect to the incoming flow. Induction control modifies the strength of the wake by adjusting the rotor thrust. Wake steering and induction control can be implemented individually, but recent studies have demonstrated the complementary benefits of joint wake steering and induction control in large eddy simulations (LES) [2].

Determining the optimal strategy for collective wind farm control requires computationally efficient models to estimate both the power production of upstream turbines as well as wake interactions and power for downstream turbines. As a turbine is yaw-misaligned, its induced velocity on the incoming flow changes, which in turn affects its power production [3]. Predicting how wake steering or induction control affects the power production of a controlled turbine requires a model of the aerodynamics at the rotor. Correspondingly, the wake of the controlled turbine also changes, which may affect the power production of turbines downwind. Far-wake models, which parameterize turbulent wake recovery, are typically used to predict the evolution of the wake downwind [4]. The rotor aerodynamics and power loss of yawed upstream turbines are often modeled with empirical (cosine) relations that are physically inconsistent with the far-wake model. Heck *et al.* [3] recently proposed a coupled approach to near- and far-wake modeling for wind farm flow control.

Inviscid near-wake models, commonly based on one-dimensional (1D) momentum theory, serve two functions: predicting the power extracted at the rotor, and the initial conditions for a far-wake model [3, 4, 5]. Commonly, these two quantities are estimated separately, using empirical fits to estimate the power loss due to yaw-misalignment with a cosine model $\cos^{\alpha}(\gamma)$, where α is a calibration parameter [6]. Calibrated $\cos^{\alpha}(\gamma)$ models have reported a wide spread of α values, highlighting that this calibration parameter depends on the turbine control strategy and wind conditions, and does not generalize across turbines or operating regimes [6, 7]. In contrast, recent physics-based near-wake models, such as that of Shapiro *et al.* [5] and Heck *et al.* [3], have proposed closures to the rotor induction based on conservation laws. Turbulent far-wake models, including the Jensen and Gaussian wake models [4], use initial conditions from a near-wake model. Commonly, the initial streamwise velocity deficit is modeled as $\delta u_0 = 2a_0$ from 1D momentum theory, where a_0 is the axial induction factor for yaw-aligned turbines. Far-wake models also require input calibration parameters, such as the wake spreading rate, that are traditionally assumed to be independent of the turbine control strategy, but this assumption has not been conclusively validated across the full range of turbine control inputs [8, 9].

Recent attention has been drawn to high-induction (thrust) rotors in the context of wake steering control. Using large eddy simulations, Cossu [10] found that high thrust rotors increased power gains due to yaw and tilt misalignment by two to three fold over standard thrust rotors. Martínez-Tossas *et al.* [9] investigated the wake recovery of yaw-aligned rotors under high thrust using LES and observed enhanced wake recovery due to increased turbulent mixing and wake contraction from a large pressure drop at the rotor. Additionally, the physics-based near-wake model of Heck *et al.* [3] predicts that increasing turbine thrust while yawing minimizes power loss due to yaw-misalignment. For these reasons, the high-thrust regime of rotor operation is of particular interest to collective wind farm flow control.

In this study, LES are performed for a partially waked two-turbine array in a conventionally neutral boundary layer (CNBL). Sweeping over a wide range of yaw and thrust coefficient values, we investigate the yaw-induction relationship for an actuator disk model (ADM) in CNBL inflow. Next, we compare the LES power production of a waked turbine to predictions from a calibrated Gaussian far-wake model [4, 5], coupled with a physics-based near-wake model [3], and we explore how wake model calibration parameters vary in different regimes of wind turbine control. Finally, we compare the power-maximizing turbine control set point for thrust and yaw between LES and the wake model predictions. With the LES data set, we explore the realizable power gain of joint yaw-induction control using a coupled wake modeling approach and identify relevant wake physics for improving steady-state far-wake models.

2 Large eddy simulation setup

Effects of joint yaw and induction control are studied using LES of a two turbine wind farm in CNBL conditions. Several calibration cases are also simulated with no downwind turbine to directly study the effects of yaw and induction control on the unimpinged wake, where the effects of induction from a downwind turbine are absent. Simulations are performed using the pseudo-spectral LES code PadéOps [11]. A Monin-Obukhov wall model is used at the bottom boundary, the sigma subgrid model computes the subgrid stresses [12], and a Rayleigh damping region is used in the top 25% of the vertical domain to absorb gravity waves. Further numerical details of the LES code can be found in Howland *et al.* [13]. All simulations use a domain $L_x = 3.84\,\mathrm{km}$, $L_y = 1.28\,\mathrm{km}$, and $L_z = 1.28\,\mathrm{km}$ in the streamwise, lateral, and wall-normal directions, respectively. A staggered grid is used with a vertical resolution of $\Delta z = 5\,\mathrm{m}$ and a horizontal resolution of $\Delta x = 10\,\mathrm{m}$ and $\Delta y = 5\,\mathrm{m}$ for a total of 25.1 million grid points. The concurrent precursor method is used [14] with a fringe region [15] in the primary simulation to replenish momentum lost to the wind turbine wake. Time-averaged statistics are collected beginning two flow-through times ($2L_x/G$) after the start of the simulation to allow transients to decay, after which flow fields and turbine power are time-averaged for two hours.

2.1 CNBL initialization

We use the procedure of Liu *et al.* [16] to initialize a CNBL. The CNBL is driven by a geostrophic wind speed of $G = 8\,\mathrm{m\,s^{-1}}$. A free atmosphere lapse rate $\Gamma = 1\,\mathrm{K\,km^{-1}}$ simulates a weakly stratified free atmosphere, and a surface roughness $z_0 = 1\,\mathrm{mm}$ is chosen to simulate offshore conditions. The CNBL spin-up simulation is run for $T = 15/f_c$, where $f_c = 1 \times 10^{-4}\,\mathrm{s^{-1}}$ is the Coriolis parameter, to allow the CNBL to reach a quasi-statistically steady state. Then, a frame angle controller is used to align the flow at hub height with the x direction [13, 17]. The CNBL which results from our spin-up simulation has a hub height wind speed $u_\infty = 7.2\,\mathrm{m\,s^{-1}}$ aligned with the x-axis. The turbulence intensity at hub height is $I_u = \sigma_u/u_\infty = 5.5\%$, where σ_u is the root-mean-square of streamwise velocity fluctuations. The wind direction changes roughly 2.2° across the rotor area due to veer caused by the Coriolis force.

2.2 Actuator disk model

The turbines are modeled as an ADM [18, 19], which imparts a forcing that depends on the disk velocity given by $\vec{F}_T = -\frac{1}{2}\rho A_d C_T' u_d^2 \hat{n}$, where ρ is air density, $A_d = \pi D^2/4$ is the disk area, $\hat{n} = \hat{\imath}\cos\gamma + \hat{\jmath}\sin\gamma$ is the normal vector to the ADM, and C_T' is the modified thrust coefficient [18]. The turbine thrust is dependent on the rotor-averaged velocity at the disk $u_d \equiv \langle \vec{u}_d \cdot \hat{n} \rangle$, where $\langle\cdot\rangle$ denotes spatial averaging over the rotor area and $\vec{u}_d$ is the velocity vector at the rotor, which is modified by induction in the LES domain. The modified thrust coefficient C_T' is used as an input instead of C_T because C_T varies with yaw (due to induction) whereas C_T' does not [3]. For a yaw-aligned turbine, following 1D momentum theory, the modified thrust coefficient is related to the standard thrust coefficient by $C_T' = C_T/(1-a_0)^2$. In yaw-misalignment, Heck *et al.* generalized the static induction factor a_0 to the rotor-normal induction $a_n(\gamma) \equiv 1 - u_d/(u_\infty \cos(\gamma))$ such that $C_T' = C_T/(1-a_n(\gamma))^2$. Here, we define $C_T = 2|\vec{F}_T|/(\rho A_d u_\infty^2 \cos^2(\gamma))$ following Shapiro *et al.* [5]. The ADM forcing kernel is smoothed by a Gaussian filtering kernel [18, 19] of width $\Delta/D = 2.5h$, where $h = (\Delta x^2 + \Delta y^2 + \Delta z^2)^{1/2}$ is the grid size. We use the ADM correction factor proposed by Shapiro *et al.* [19].

2.3 Single turbine calibration simulations

We first describe a single-turbine LES simulation to study the wake behavior in absence of downstream turbines. One advantage of studying the unimpinged wake is that the accuracy of the wake model to predict the velocity field downwind can be studied separately from the accuracy of the model's predictions for power downwind, which will depend on interaction between the rotor induction and the incident wind field. We use the single-turbine simulations for wake model calibration. A single turbine of diameter $D = 100\,\mathrm{m}$ is placed $x = 5D$ from the inlet of the domain, centered laterally, at a hub height of $z_h = 100\,\mathrm{m}$. An independent value of the local thrust coefficient C_T' and the yaw angle γ are prescribed to the leading turbine only and are constant in time such that each simulation is statistically steady. In the calibration simulations, the lone turbine is yawed between $\gamma_1 \in [0^\circ, 30^\circ]$ and the thrust coefficient is modified between $C_{T,1}' \in [0.8, 4.0]$.

2.4 Wind farm simulations

In wind farm simulations, two turbines with diameters of $D = 100\,\mathrm{m}$ are immersed in the CNBL. A turbine is placed in the wake of the leading turbine with streamwise and lateral spacing $S_x = 6D$ and $S_y = 0.4D$, respectively. The lateral offset S_y creates partial waking which favors positive yaw-misalignments (anti-clockwise viewed from above). In the wind farm simulations, the leading turbine is yawed between $\gamma_1 \in [0^\circ, 45^\circ]$ and the thrust coefficient is modified between $C_{T,1}' \in [0.4, 4.0]$. The waked turbine, which has no downstream turbines, operates at the power-maximizing set point $C_{T,2}' = 2.0$ and $\gamma_2 = 0^\circ$ as predicted by yaw-aligned momentum theory (Betz limit set point). The control set points of both turbines do not change in time during each simulation. A schematic for the wind farm setup is shown in Figure 1.

3 Wake modeling methodology

In this section, we outline the wake modeling framework. We use a variant of the Gaussian far-wake model initially derived by Bastankhah and Porté-Agel [4] and extended by Shapiro *et al.* [5]. The far-wake model uses an initial condition from a near-wake model, which predicts the streamwise and spanwise wake velocity deficits, as well as the rotor induction and power.

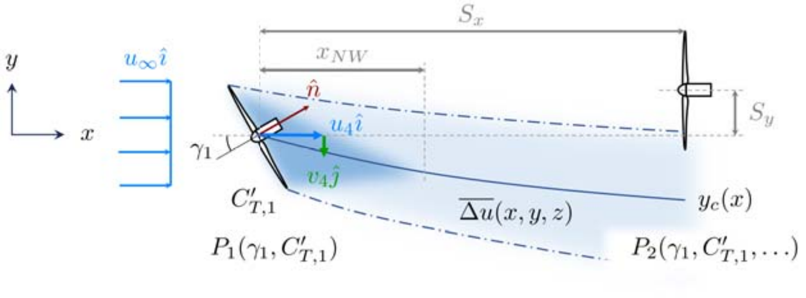

Figure 1: A schematic of the two-turbine configuration with turbine spacing $S_x = 6D$ and $S_y = 0.4D$. The leading turbine is controlled while the waked turbine operates at the Betz limit ($\gamma_2 = 0, C'_{T,2} = 2.0$).

3.1 Near wake modeling

To model the near-wake behavior, we use the near-wake (inviscid) model of Heck *et al.* [3], which extends on the work of Shapiro *et al.* [5]. The velocity at the rotor, which is modified by induction, is dependent on the thrust and yaw of the wind turbine. By applying conservation of mass, momentum, and energy, the model introduced by Heck *et al.* predicts the rotor-normal, rotor-averaged induction $a_n(\gamma)$ and streamwise and spanwise outlet velocities u_4 and v_4, respectively. The near-wake model (Eq. (2.15) in Heck *et al.*) takes independent inputs of yaw-misalignment angle γ and thrust coefficient C'_T to solve the coupled, non-linear system of three equations.

The induction $a_n(\gamma)$ is used to compute the turbine power

$$P \equiv -\vec{F}_T \cdot \vec{u}_d = \frac{1}{2}\rho A_d C'_T u_\infty^3 \cos^3(\gamma)(1 - a_n(\gamma))^3, \tag{1}$$

while the wake strength and deflection depend on the initial wake velocities u_4 and v_4.

3.2 Far-wake modeling

In the far-wake of a yaw-aligned turbine, wake velocities become self-similar and Gaussian in shape [4]. We assume that the time-averaged wake velocity deficit $\overline{\Delta u}(x, y, z) \equiv u_\infty - \bar{u}(x, y, z)$ is Gaussian and expands linearly beginning at the near-wake length x_{NW} [8, 5].

In this work, we extend the Gaussian wake model proposed by Shapiro *et al.* [5]. Beginning with the linearized Navier–Stokes equations, they proposed a model for the wake deficit field:

$$\overline{\Delta u}(x, y, z) = \delta u(x) \frac{D^2}{8\sigma_0^2} \exp\left(-\frac{(y - y_c(x))^2 + (z - z_h)^2}{2\sigma_0^2(x) d_w^2(x)}\right). \tag{2}$$

Here, σ_0 is the initial wake width at $x = 0$, $d_w(x) = 1 + k_w \ln(1 + \exp[2(x - x_{NW})/D])$ is an effective wake diameter, and y_c is the wake deflection. As suggested in Bastankhah and Porté-Agel [8], we fix the value $\sigma_0 = D/\sqrt{8}$. Note that for this value of σ_0, the wake-averaged velocity deficit $\delta u(x)$ is equal to the maximum wake velocity deficit. The function $d_w(x)$ approaches 1 near the turbine and transitions smoothly to a linear expansion of slope $2k_w$ beyond $x \sim x_{NW}$, where k_w is a calibration parameter for the wake spreading rate. While Shapiro *et al.* originally proposed fixing $x_{NW} = D$, we will investigate the importance of modeling the near-wake length for a wide range of thrust coefficients. The near-wake closure for x_{NW}, adapted from Bastankhah and Porté-Agel [8], is given by

$$\frac{x_{NW}}{D} = \frac{\cos(\gamma)\left[1 + \sqrt{1 - C'_T(1 - a_n(\gamma))^2 \cos^2(\gamma)}\right]}{\sqrt{2}\left[\alpha^* I_u + \beta^*(1 - \sqrt{1 - C'_T(1 - a_n(\gamma))^2 \cos^2(\gamma)})\right]}, \tag{3}$$

where $\alpha^* = 2.32$ and $\beta^* = 0.154$ are recommended by Bastankhah and Porté-Agel [8]. The near-wake length can be interpreted as a virtual origin for the far-wake model, which improves predictions of the wake velocity field [20].

The wake velocity deficit function $\delta u(x)$ is modeled as a smoothed step function in the vicinity of the rotor, and the lateral velocity is modeled similarly:

$$\delta u(x) = \frac{u_\infty - u_4}{d_w^2(x)} \frac{1}{2}\left[1 + \operatorname{erf}\left(\frac{x}{\sqrt{2}D/2}\right)\right]; \quad \delta v(x) = \frac{-v_4}{d_w^2(x)} \frac{1}{2}\left[1 + \operatorname{erf}\left(\frac{x}{\sqrt{2}D/2}\right)\right], \tag{4}$$

where u_4 and v_4 are initial wake velocities from the near-wake model [3]. Finally, the wake deflection is computed by numerically integrating $\delta v(x)$ from (4) in the x-direction such that

$$y_c(x) = \int_0^x \frac{-\delta v(x')}{u_\infty} \,\mathrm{d}x'. \tag{5}$$

No wake superposition method is needed because the downstream turbine wake is not relevant in this study. Adding additional rows of turbines would require modeling deep array effects, including secondary steering and wake-added turbulence intensity.

The power of the waked turbine is affected by the wake of the upstream turbine. In the actuator disk formulation, power is proportional to the cube of the rotor-averaged wind speed u_d. To compute the power production of the waked turbine, we modify u_∞ in (1) to include wakes of upstream turbines. The rotor-averaged wake deficit $\langle\overline{\Delta u}\rangle$ is subtracted from the freestream flow such that $u_{\infty,2} = u_\infty - \langle\overline{\Delta u}\rangle$. We compute the waked turbine power using $\overline{\Delta u}$ from the wake model and the momentum theory-based induction closure of Heck *et al.* discussed in Section 3.1.

3.3 Wake model calibration

Wake models incur error from the model form, as well as from calibration parameters. To minimize the error resulting from model parameters, we opt to calibrate the coupled wake model introduced in Sections 3.1 and 3.2 directly to the single-turbine LES velocity field. Because turbine power depends on the rotor-averaged wind speed, we choose a three-dimensional domain to calibrate the far wake model. We minimize the mean absolute error between the wake modeled velocity deficit field and the LES deficit field, computed by subtracting the time-averaged base flow in the precursor simulation from the time-averaged flow field including a turbine wake. The calibration region we choose centers around the downwind turbine such that $x \in [S_x - D, S_x + D]$, $y \in [-2D, 2D]$, $z \in [z_h - D, z_h + D]$. The Broyden–Fletcher–Goldfarb–Shanno algorithm [21] is used in the `scipy.optimize` package to find the optimal calibration parameter k_w.

4 Results

In this section, we compare rotor induction and wake velocities from LES with the near-wake model. Then, we examine the far-wake behavior in LES. Finally, we calibrate a Gaussian wake model to the yaw-aligned LES data, and use the calibrated wake data to predict the optimal thrust and yaw of the two-turbine system.

4.1 Near-wake characteristics

Near-wake properties are shown in Figure 2 as computed from LES data. Both the calibration (one-turbine, solid plus +) and wind farm (two-turbine, open circle ∘) simulations are used because the presence of the downwind turbine has only a small effect on the near-wake characteristics. We compute $\delta u_0 = u_\infty - u_4$ from LES as the maximum value of the wake velocity deficit field $(\overline{\Delta u})$. Defining δu_0 based on the maximum value from the LES velocity deficit field is useful because the wake strength in the Gaussian wake model (2) depends on the maximum velocity deficit $\delta u(x)$. The initial lateral velocity component δv_0 is computed by streamtube-averaging $(\langle\cdot\rangle_s)$ the lateral velocity deficit $\langle\overline{\Delta v}\rangle_s$ in the yz-plane. The streamtube is seeded at the ADM at a radius $R_s = 0.35D$, but results are relatively insensitive to the initial streamtube seeding position. This is the same approach to identify δv_0 as in Shapiro *et al.* [5]. The induction factor a_n is computed from LES using the rotor-averaged disk velocity u_d which includes the ADM correction factor [19].

The rotor-normal induction factor, shown in Figure 2(a), increases with increasing turbine thrust and decreases with increasing yaw-misalignment magnitude. Overall, the trends for a_n in the CNBL LES are similar to those reported in Heck *et al.* for uniform inflow [3]. Predictions of the induction factor, which are important for predicting the power of the upstream turbine, show good agreement with LES up to $\gamma_1 \approx 30^\circ$. The modeled induction factor a_n decreases in accuracy for increasing thrust coefficient due to the presence of a non-negligible wake base pressure [9, 22]. The effect of the wake base pressure decreases the induction and, by extension, decreases the streamwise velocity deficit δu_0.

Wake streamwise velocity deficit δu_0 in Figure 2(b) matches momentum theory predictions for yaw-aligned wakes up to $C'_{T,1} \approx 2$. Additionally, for constant $C'_{T,1}$, increasing the magnitude of yaw misalignment decreases the wake strength. For high thrust rotors $C'_{T,1} > 2$, an overestimation of δu_0 is observed in the model, which is associated with increased model error in the induction stemming from the wake base pressure. For low thrust coefficients (e.g., $C'_{T,1} = 0.8$), overestimation of δu_0 in the wind

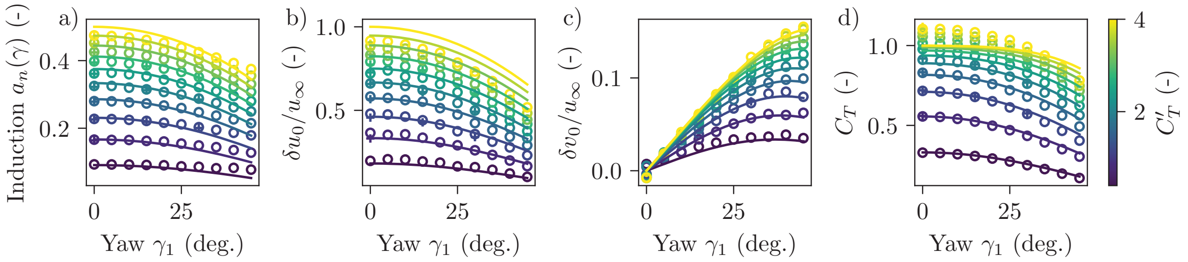

Figure 2: (a) Rotor-normal, rotor-averaged induction factor a_n and near-wake velocity deficits in the (b) streamwise and (c) lateral directions, and (d) thrust coefficient C_T. Solid plus + symbols represent data from single turbine calibration simulations, open circles ∘ are from wind farm simulations, and model predictions are shown with solid lines.

farm simulations is due to the presence of the induction zone from the waked turbine given the large near-wake length (Section 4.2). The initial lateral wake velocity deficit δv_0 increases in magnitude with increasing thrust and increasing yaw misalignment angle, as is shown in Figure 2(c). Overall, predictions of δv_0 from the near-wake model are in excellent agreement with LES data, even for high yaw-misalignment angles $\gamma_1 = 45^\circ$ and for high thrust coefficients $C_{T,1}' > 2$. Finally, in Figure 2(d), we show C_T as a function of C_T' and yaw. As thrust increases ($C_T' > 3$), the model increasingly underpredicts C_T as a result of the overprediction in static induction a_n. The underprediction of thrust in the near-wake model from Heck *et al.* is a persistent challenge for high thrust rotors which is commonly addressed in blade-element momentum methods with empirical corrections [23]. Improved modeling of the high-thrust regime should be explored in future work to improve near-wake modeling.

4.2 Far-wake characteristics

In this section, we focus on far-wake analysis using the one turbine calibration data. The underlying hypothesis is that accurately predicting the wake velocity field will lead to accurate predictions of the waked turbine power. The maximum wake deficit from LES as a function of downstream distance x is shown in Figure 3(a) for the yaw-aligned $\gamma_1 = 0^\circ$ calibration simulations.

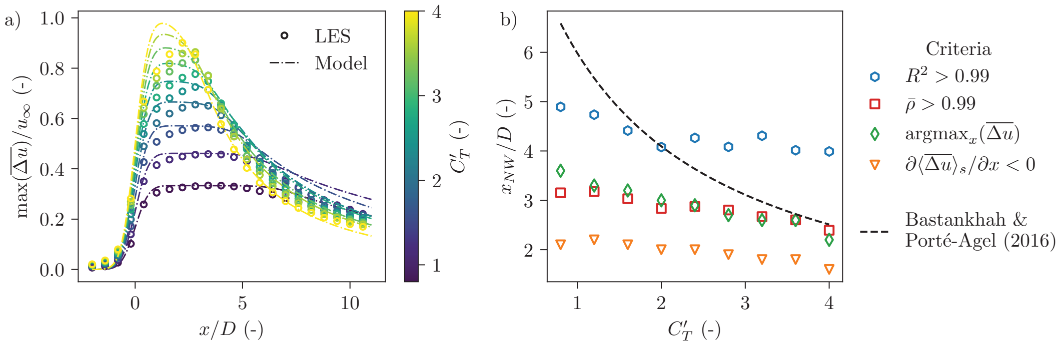

Figure 3: Yaw-aligned wake characteristics, including (a) maximum wake deficit $\overline{\Delta u}$ as a function of downstream distance for wake model predictions (dashed lines) and LES (open circles ∘) and (b) near-wake length x_{NW} as a function of thrust coefficient.

The maximum streamwise wake velocity deficit, which is related to the near-wake velocity (Figure 2(b)), increases as the rotor thrust increases. However, the monotonic trend observed in $\max(\overline{\Delta u})$ for $x < 2D$ does not generally hold for all downstream locations x. Instead, we find that the rapid wake recovery rate at the highest turbine thrust breaks the monotonicity in $\max(\overline{\Delta u})$ before $x = 5D$. By $x = 8D$, the highest thrust turbine produces the wake with the smallest maximum velocity deficit. The rotor-averaged velocity of a ghost turbine in the wake of the freestream turbine also shows

shows non-monotonic behavior due to the enhanced wake recovery from the high thrust region (not shown). This observation is contrary to the traditional approach of induction control, where leading turbines curtail power by decreasing thrust in an attempt to decrease the strength of the wake interfering with downwind turbines. Instead, the LES data shows that an alternative to decreasing wake strength downwind could be to increase the rotor thrust—promoting wake recovery—if the waked turbine is sufficiently far downwind.

The non-monotonic behavior of the maximum wake strength is the result of two mechanisms. First, the near-wake length x_{NW} decreases, as is shown visually in Figure 3(a) by the location where the wake strength begins to decrease. This point is marked by the green diamonds in Figure 3(b). Other methods of measuring the near wake length x_{NW} are compared in Figure 3(b). These include the downstream location where the R^2 value [24] or Pearson correlation coefficient $\bar{\rho}$ [25] of the best-fit Gaussian profile compared to a wake transect at hub height exceeds 0.99 and the location where the streamtube-averaged wake $\langle\overline{\Delta u}\rangle_s$ begins to recover. The near-wake length closure model is also included in Figure 3 [8]. While different definitions of x_{NW} show different quantitative results, all definitions of x_{NW} show a decreasing near-wake length as rotor thrust C_T' increases. The near-wake length demarcates the boundary between the inviscid region of wake expansion and the turbulent region of wake recovery. As x_{NW} decreases, the onset of the turbulent wake (and region of wake recovery) occurs closer to the rotor. Therefore, as rotor thrust increases, the wake velocity has more distance (time) to recover before it reaches the downwind turbine.

In addition to the decreasing near-wake length is the increased rate of turbulent wake recovery with increasing rotor thrust. While Martínez-Tossas *et al.* [9] observed enhanced wake recovery for high ($C_T > 1$, i.e., $C_T' > 4$) rotor thrust coefficients in yaw-aligned uniform inflow, we observe that the wake recovery rate continuously increases as C_T' increases, as shown in Figure 3(a). The decrease in near-wake length and enhanced wake recovery with increasing C_T' are both driven by increasing the shear-generated turbulence to replenish momentum into the wake [8, 24]. In summary, high-induction operation is favored for joint yaw-induction control in three ways: 1) power loss due to yaw misalignment is partially mitigated by increasing the leading turbine thrust [3], 2) wake deflection increases as thrust increases, and 3) wake recovery rates increase with increasing thrust.

4.3 Model calibration

The far-wake model is calibrated to LES data using initial wake velocities from the near-wake model of Heck *et al.* As noted in Section 4.2, the wake recovery rate, which is related to the wake spreading parameter k_w, changes as a function of thrust. Results of the model calibration are shown in Figure 4.

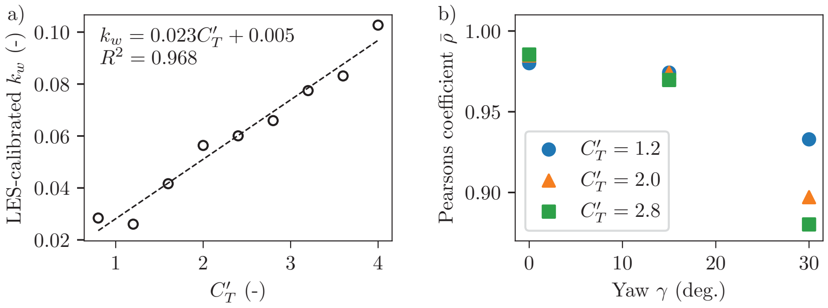

Figure 4: (a) Calibration for the wake spreading parameter k_w using yaw-aligned LES velocity fields. (b) Pearsons correlation coefficient for velocity field fit under yaw-misalignment.

The wake spreading rate k_w varies significantly with across the range of simulated C_T', as shown in Figure 4(a). For an initial approximation, we fit a least-squares linear regression through the data to approximate the dependence of k_w on thrust, although this trend likely depends on atmospheric conditions and rotor modeling. Other parameterizations for the dependence of k_w on thrust have also been proposed (e.g., Ishihara and Qian [26]).

Figure 4(b) shows the Pearsons correlation coefficient between the wake model field and LES wake deficit field in the calibration region. In yaw-misalignment, the model-form error of the Gaussian wake model increases due to wake curling [8, 27]. In addition, increasing turbine thrust increases the wake deflection and wake curling, increasing the error between LES and the best-fit Gaussian wake model velocity field. As a result, wake calibration in yaw-misalignment leads to inaccurate estimates for k_w. Wake spreading rate, as measured in hub height wake velocity fields, is not strongly dependent on yaw (not shown), as was noted previously by Bastankhah and Porté-Agel [8]. Therefore we choose to calibrate k_w to each yaw-aligned wake as a function of C_T' only. The dependence of k_w on C_T' in Figure 4(a) will be compared with a far-wake model using constant k_w, corresponding with $C_T' = 2.0$, in Section 4.4.

4.4 Model power predictions

We compare LES results and model predictions for the efficiency of the upstream turbine and total farm efficiency $\eta_{tot.} = (\eta_1 + \eta_2)/2$ in Figure 5, where $\eta_i = 2P_i/(\rho A_d u_\infty^3)$. The Coupled model uses the induction closure of Heck *et al.* to compute power, while the Cosine model assumes a relationship $P(\gamma)/P(\gamma = 0) = \cos^\alpha(\gamma)$. Here, the parameter $\alpha = 1.98$ is calibrated to the LES data at $C_T' = 2.0$. Although the Cosine model is calibrated to LES data, while the model of Heck *et al.* is parameter-free, predictions of η_1 from the cosine model have higher error than the model of Heck *et al.* when considering the full range of C_T'. This is because the power lost due to yaw-misalignment is dependent on thrust [3]. In both models, we use the same far-wake model where $x_{NW} = 3D$ is fixed, and k_w is calibrated to the single-turbine data at $C_T' = 2.0, \gamma = 0°$. We find that the variable near-wake length and variable wake spreading rate $k_w(C_T')$ do not improve predictions of waked turbine efficiency η_2, relative to LES, when the leading turbine is yaw-misaligned. This result is due to a combination of factors. First, the wake curling induced by high yaw γ_1 (Figure 4(b)) causes the wake to curl around the downwind turbine as yaw-misalignment is increased. Neglecting the wake curling results in an overprediction of the wake strength on the downwind turbine and an underprediction of the waked turbine power. In addition, the error of the initial streamwise velocity deficit δu_0 increases with increasing rotor thrust $C_{T,1}'$ (Figure 2(b)). The model overprediction of δu_0 may be biasing the model calibration and therefore the functional dependence of $k_w(C_T')$. However, we emphasize that the increased wake recovery as a function of increasing C_T' is a result that is robust to any potential calibration bias, as shown in Figure 3(a). Finally, we note that the quantitative trends predicted by the near-wake length model (3) do not follow trends in the LES. For example, the model predicts that increasing the yaw-misalignment angle will increase the near-wake length, while we observe x_{NW} decreasing with increasing yaw-misalignment in the LES data (not shown). The quantitative sensitivity of choices in the far-wake modeling on $\eta_{tot.}$ is shown in Table 1.

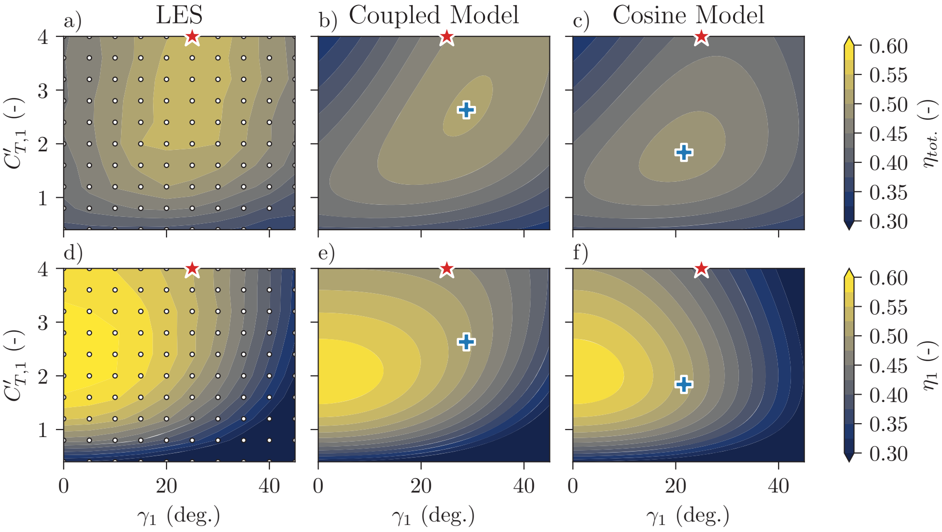

Figure 5: Contours of (a-c) total farm efficiency and (d-f) upstream turbine efficiency η_1 for LES, the coupled near-wake model from Heck *et al.*, and a cosine power loss model calibrated to $C_{T,1}' = 2.0$. Blue + markers denote the set point corresponding with the modeled maximum farm efficiency and red $\star$ markers denote the power-maximizing LES set point.

The wake models are used to predict optimal set points for wind farm flow control. The farm power-maximizing set point is denoted with a marker on each plot. The resulting optimal set point predicted by the Coupled model lies closer to the LES optimal than when using the Cosine model. In LES, the power-maximizing set point is $C'_{T,1} = 4.0$, $\gamma_1 = 25°$. We note that because the LES power-maximizing thrust is on the border of the values simulated here, it is possible that the true optimal thrust is $C'_{T,1} > 4.0$, and future studies should investigate the true optimal with more supercomputer availability. Regardless, the LES optimal control strategy indicates $C_{T,1}$ should be increased, compared to standard control ($C'_T = 2$), rather than decreased. This is captured by the near-wake model from Heck *et al.* but not by a calibrated Cosine model.

Table 1 summarizes the accuracy of the different wake model predictions. The baseline strategy assumes standard control where turbines are yaw-aligned and operate at the Betz limit ($C'_{T,1} = 2$). The column labeled LES-equivalent ("LES eq. $\eta_{tot.}$") is computed by interpolating the LES data at the model-optimal control set point. When the physics-based near-wake model of Heck *et al.* is used, the optimal C'_T exceeds the Betz limit thrust coefficient recommendation. The power gain at at the optimal set point is 20.7% above baseline in the LES data. The near-wake model of Heck *et al.* predicts a power gain of approximately 18% depending on the far-wake model, while the calibrated Cosine model predicts a 13.7% power gain. Finally, using the optimal physics-based model set point in LES results in a farm power within 1.5% of the true optimal farm power in LES.

Table 1: Optimal set point $(\gamma_1, C'_{T,1})$ to maximize array efficiency $\eta_{tot.}$ for LES and wake models. The column "LES eq." is the LES farm efficiency interpolated at the model-predicted optimal set point.

Near-wake	**Far-wake**	**Optimal** γ_1 (°)	**Optimal** C'_T	**Baseline** $\eta_{tot.}$	**Optimized** $\eta_{tot.}$	**Gain** **(%)**	**LES eq.** $\eta_{tot.}$
(LES)	(LES)	25	4.0	0.447	0.538	20.7	0.539
Heck *et al.*	Fixed x_{NW}	29	2.6	0.425	0.497	18.1	0.530
Heck *et al.*	Variable x_{NW}	27	2.2	0.426	0.503	18.1	0.530
Heck *et al.*	Variable x_{NW}, k_w	26	2.1	0.424	0.503	18.8	0.529
Cosine model	Fixed x_{NW}	22	1.8	0.426	0.486	13.5	0.520
Cosine model	Variable x_{NW}	22	1.8	0.424	0.486	13.7	0.520

5 Discussion and Conclusions

In this study, we investigate the power maximization of a two-turbine wind farm array in partially waked conditions through joint wake steering-induction control. Using large eddy simulations of a small wind farm in a conventionally neutral boundary layer, we sweep over a wide range of yaw and thrust control inputs, highlighting the high thrust region of operation. While the general approach for turbine operation is to keep the rotor thrust below the Betz optimum ($C_T = 8/9$ or $C'_T = 2.0$) to reduce the velocity deficit strength of wakes downstream, we observe three benefits for operating in the high-thrust regime in the context of wind farm flow control. First, power loss due to yaw-misalignment of the leading turbine is partially mitigated by compensatory increases in turbine thrust. Additionally, higher turbine thrust results in a larger initial lateral velocity downwind of yawed turbines and, by extension, larger wake deflection. Finally, we observe that as rotor thrust increases, the near-wake length decreases and the wake recovery rate increases as a result of enhanced shear-generated turbulence, leading to faster wake recovery. Large eddy simulations of a two-turbine array result in a power-maximizing thrust of $C'_{T,1} = 4.0$ and yaw $\gamma_1 = 25°$ for the leading turbine. While the magnitude of the optimal rotor thrust will depend on the array configuration, atmospheric characteristics, and rotor aerodynamics, this result suggests future research into the wake dynamics and modeling of high-thrust rotors.

Computationally efficient models are necessary for predicting the optimal wind turbine control strategy. Here, we introduce a coupled wake model which uses the near-wake model of Heck *et al.* as an initial condition for a Gaussian far wake model. The wake model captures the power-maximizing wind farm control strategy with lower error than a calibrated cosine model. However, the near-wake model degrades in accuracy as rotor thrust is increased, which is related to the wake base pressure for highly-loaded rotors [22]. As a result, the near-wake model underpredicts the power produced by the upstream turbine and overpredicts the wake deficit magnitude under high thrust conditions. We hypothesize that improved near-wake modeling in high-thrust conditions will improve predictions of wind farm power and power maximizing control set points over current models, when compared with LES. Additionally, we find that current models for the near-wake length x_{NW} for turbines in yawed conditions do not quantitatively predict the near-wake length with enough accuracy to improve predictions of the power-maximizing set point over assuming a fixed value of x_{NW}. Improved models for the near-wake length can improve far-wake modeling in the coupled wake modeling framework. Finally, future work into induction modeling under sheared and partially waked conditions and improvements in modeling wake turbulence and curling will continue to improve the accuracy of wake models for wind farm flow control applications.

Acknowledgements

K.S.H. and M.F.H. acknowledge funding from the National Science Foundation (Fluid Dynamics program, grant number FD-2226053, Program Manager: Dr. Ronald D. Joslin). K.S.H. acknowledges additional funding from a National Science Foundation Graduate Research Fellowship under grant no. DGE-2141064. J.L. acknowledges support from Siemens Gamesa Renewable Energy. Simulations were performed on the Stampede2 and Stampede3 supercomputers under the NSF ACCESS project ATM170028.

References

[1] Meyers J, Bottasso C, Dykes K, Fleming P, Gebraad P, Giebel G, Göçmen T, van Wingerden J W 2022 *Wind Energy Sci.* **7** 2271-2306
[2] Munters W and Meyers J 2018 *Energies* **11** 177
[3] Heck K S, Johlas H M, and Howland M F 2023 *J. Fluid Mech.* **959** A9
[4] Bastankhah M and Porté-Agel F 2014 *Renew. Energy* **70** 116-123
[5] Shapiro C R, Gayme D F, and Meneveau C 2018 *J. Fluid Mech.* **841** R1
[6] Liew J, Urbán A M, Andersen S J 2020 *Wind Energy Sci.* **5** 427-437
[7] Howland M F, González C M, Martínez J J P, Quesada J B, Larrañaga F P, Yadav N K, Chawla J S, Dabiri J O 2020 *J. Renew. Sustain. Energy* **12** 063307
[8] Bastankhah M and Porté-Agel F 2016 *J. Fluid Mech.* **806** 506-541
[9] Martínez-Tossas L A, Branlard E, Shaler K, Vijayakumar G, Ananthan S, Sakievich P, and Jonkman J 2022 *Wind Energy* **25** 605-617
[10] Cossu C 2021 *Wind Energy Sci.* **6** 377-388
[11] Ghate A S and Lele S K 2017 *J. Fluid Mech.* **819** 494-539
[12] Nicoud F, Toda H B, Cabrit O, Bose S, Lee J 2011 *Phys. of Fluids* **23** 085106
[13] Howland M F, Ghate A S, and Lele S K 2020 *J. Fluid Mech.* **883** A39
[14] Stevens R JAM, Graham J, and Meneveau C 2014 *Renew. Energy* **68** 46-50
[15] Nordström J, Nordin N, Henningson D 1999 *SIAM J. Sci. Comput.* **20** 1365-1393
[16] Liu L, Gadde S N, and Stevens R JAM 2021 *Q. J. R. Meteorol. Soc.* **147** 847-857
[17] Sescu A and Meneveau C 2014 *Q. J. R. Meteorol. Soc.* **140** 2017-2022
[18] Calaf M, Meneveau C, and Meyers J 2010 *Phys. Fluids* **22** 015110
[19] Shapiro C R, Gayme D F, and Meneveau C 2019 *Wind Energy* **22** 1414-1420
[20] Neunaber, I, Hölling, M, and Obligado, M 2024 *Renew. Energy* **223** 119935
[21] Nocedal J and Wright S J 2006 Numerical Optimization Springer New York
[22] Liew, J, Heck, K S, and Howland, M F 2024 *arXiv preprint* arXiv:2401.09623
[23] Moriarty P J and Hansen A C 2005 Aerodyn theory manual *Tech. rep.* NREL/TP-500-36881, 15014831
[24] Vahidi D and Porté-Agel F 2022 *J. Fluid Mech.* **943** A49
[25] Sørensen J N, Mikkelsen R F, Henningson D S, Ivanell S, Sarmast S, Andersen S J 2015 *Phil. Trans. R. Soc.* **A 373** 20140071
[26] Ishihara T and Qian G W 2018 *J. Wind. Eng. Ind. Aerodyn.* **177** 275-292
[27] Howland M F, Bossuyt J, Martínez-Tossas L A, Meyers J, and Meneveau C 2016 *J. Renew. Sustain. Energy* **8** 043301
[28] Martínez-Tossas L A, King J, Quon E, Bay C J, Mudafort R, Hamilton N, Howland M F, and Fleming P A 2021 *Wind Energy Sci.* **6** 555-570